On the stability of two-derivative time discretizations

A. Thenery Manikantan, J. Zeifang and J. Schütz

UHasselt Computational Mathematics Preprint Nr. UP-23-02

August 4th, 2025

On the stability of two-derivative time discretizations

Arjun Thenery Manikantan*, Jonas Zeifang†, Jochen Schütz‡

Abstract

In this paper, we analyze stability properties of the two-derivative strong stability preserving schemes presented in [Gottlieb et al., SIAM Journal on Numerical Analysis 60, 2022]. Stability analysis shows that the diagonally implicit two-derivative two-stage third-order strong stability preserving scheme can never be A-stable. We provide a detailed investigation of the third-order schemes and discuss stabilizing strategies. The stabilizing techniques are applicable to tune any general implicit two-derivative scheme. We implement the two-derivative strong stability preserving schemes for partial differential equations with a discontinuous Galerkin spectral element spatial discretization. We use Newton's method for non-linear stage equations and the generalized minimal residual method with a matrix-free approach for solving linear algebraic equations under suitable preconditioning. The method is applied for compressible Euler and Navier-Stokes equations with orders up to four. Numerical results show that the second and fourth-order strong stability preserving schemes attain their desired order of convergence for relatively large timesteps. In contrast, third-order schemes require smaller timesteps to exhibit convergence. Nevertheless, the improved adaptive third-order scheme yields stable solutions.

Keywords: Strong stability preserving; Implicit time stepping; Multiderivative schemes; Stability analysis; Discontinuous Galerkin spectral element method

AMS Subject Classification: 65L05; 65M20; 65M22; 65M60

1 Introduction

Consider the partial differential equations (PDE) defined on the spatial domain $\Omega \subset \mathbb{R}^n$,

$$\mathbf{w}_t + \nabla \cdot \mathbf{F}(\mathbf{w}) = 0, \tag{1}$$

where $\mathbf{w}(x,t) : \Omega \times \mathbb{R}_{\geq 0} \to \mathbb{R}^m$ is the state vector and $\mathbf{F}(\mathbf{w}) : \mathbb{R}^m \to \mathbb{R}^m$ is the flux. For the Navier-Stokes equation, the flux function is given by

$$\mathbf{F}(\mathbf{w}) := \mathbf{F}^{\text{inv}}(\mathbf{w}) - \mathbf{F}^{\nu}(\mathbf{w}, \nabla \mathbf{w}), \tag{2}$$

with the inviscid flux $\mathbf{F}^{\text{inv}}$ and the viscous flux $\mathbf{F}^{\nu}$, where fluxes are given in Eqs. (38) and (41) below. The Euler equations are obtained by setting $\mathbf{F}^{\nu} \equiv 0$ in Eq. (2). Formally, the PDE (1) can be cast into an ordinary differential equation (ODE)

$$\mathbf{w}_t = \mathbf{R}^{(1)}(\mathbf{w}) \tag{3}$$

in some infinite dimensional function space, where the function $\mathbf{R}^{(1)}(\mathbf{w})$ is defined as

$$\mathbf{R}^{(1)}(\mathbf{w}) := -\nabla \cdot \mathbf{F}(\mathbf{w}). \tag{4}$$

*arjun.thenerymanikantan@uhasselt.be, Faculty of Sciences & Data Science Institute, UHasselt, Belgium
†jonas.zeifang@uhasselt.be, Faculty of Sciences & Data Science Institute, UHasselt, Belgium
‡jochen.schuetz@uhasselt.be, Faculty of Sciences & Data Science Institute, UHasselt, Belgium

Widely used time stepping methods in the field of compressible computational fluid dynamics are of explicit nature. However, the conditional stability of the explicit integration schemes imposes timestep restrictions, which arise from the CFL condition. In order to overcome these timestep restrictions, we use *implicit time stepping schemes* which have less severe or no restrictions on the timestep. Multistep methods such as backward difference formulae (BDF) or multistage methods such as diagonally implicit Runge-Kutta (DIRK) methods are standard examples for implicit time stepping methods. In [12], some efficient implicit schemes based on Rosenbrock Runge-Kutta methods [2] and BDF methods can be found.

Classical implicit time stepping schemes in literature mostly use only the first-order derivative ($\mathbf{w}_t$) for temporal integration [12]. The consistency order of one-derivative Runge-Kutta methods can only be improved by increasing the number of stages; this requires additional memory and necessitates solving more involved order conditions. To overcome this situation, one can include higher-order derivatives in the time stepping procedure, resulting in *multiderivative methods*. The multistage multiderivative schemes were first considered half a century ago in [29, 28, 10]. In general, these methods belong to the larger class of multistep-multistage-multiderivative methods [10]. Including higher order derivatives in time stepping gives more flexibility to the method; hence it can achieve higher orders of consistency with the same number of stages as used in the one-derivative schemes [28, 4]. This current work is limited to only *two-derivative schemes*. Hence it is required to compute also the second-order derivative for the temporal integration,

$$\mathbf{w}_{tt} = (\mathbf{R}^{(1)}(\mathbf{w}))_t = -\nabla \cdot \left(\frac{\partial \mathbf{F}}{\partial \mathbf{w}}(\mathbf{w}) \mathbf{R}^{(1)}(\mathbf{w}) \right) := \mathbf{R}^{(2)}(\mathbf{w}, \mathbf{R}^{(1)}(\mathbf{w})). \tag{5}$$

An asymptotic preserving higher-order implicit two-derivative method for stiff ODEs was developed in a predictor-corrector fashion [25, 27], termed Hermite-Birkhoff Predictor-Corrector schemes (HBPC). In each correction step, the order of consistency is raised by one until some maximal order is reached; order reduction for low stiffness parameters was mitigated by adding more correction steps. The HBPC scheme was optimized in [30] to have $A(\alpha)$ stability almost up to $\alpha = 90^o$.

In [7], Gottlieb et al. developed a higher-order implicit two-derivative Runge-Kutta-type scheme that possesses the strong stability preserving (SSP) property. Refer to [8, 5, 9] for more two-derivative SSP schemes. Besides multistage methods, there are higher-order SSP two-derivative general linear methods in literature, see, e.g. [23]. In [5, 9], explicit two-derivative SSP schemes are combined with weighted essentially non-oscillatory methods to solve conservation laws. Applications of implicit multiderivative methods combined with discontinuous Galerkin spatial discretization for (non-)linear PDEs can be found in [26, 14, 24]. In [31], the HPBC schemes [25, 27] are combined with discontinuous Galerkin spectral element method (DGSEM) [17] and achieve order of accuracy up to eight. The scheme is parallelized in space and in [32] also in time.

In this work, we combine the two-derivative implicit SSP [7] time discretization approach with a spatial discretization of the DGSEM to solve Navier-Stokes equations. Linear stability properties of the SSP schemes [7] are investigated. A detailed stability analysis of the third-order SSP scheme is conducted, and several stabilizing strategies are discussed. We leverage the flexibility of two-derivative schemes, which allows for tuning the positions of the poles of the stability function, to enhance the stability of our scheme. As a result, we derive a family of A(α)-stable third-order SSP schemes and implement them in an adaptive manner to provide stable solutions. The implicit stages of the discretized system are solved using Newton's method and the generalized minimal residual method (GMRES) is used with appropriate preconditioning to solve the linear system arising in the Newton iterations. As the SSP schemes are structurally very similar to the stages of the HBPC schemes, we closely follow the preconditioning and the matrix-free approach implemented in [31].

The sections of this paper are structured as follows: In Sec. 2 the semi-descretization of the two-derivative SSP schemes are explained with Butcher form, followed by the investigation of the stability properties. The fully discrete formulation is briefed in Sec. 3 with the weak formulation of the PDEs. Effect of preconditioning and the

implementation of the preconditioner using a matrix-free approach is shortly recalled in Sec. 3.2. In Sec. 4.1.1, a detailed analysis of the third-order schemes is conducted, and adaptive schemes are derived to enhance stability properties. The validation of the SSP schemes on Euler and Navier-Stokes equations is presented in Secs. 4.2 and 4.3, including convergence results and statistics of the number of (non-)linear iterations. In the final section (Sec. 5), conclusions are made and an outlook is given.

2 Semi-discrete formulation

In this section, we discuss the semi-discrete formulation of the implicit two-derivative SSP Runge-Kutta method. We use the spatial operators $\mathbf{R}^{(1)}$ and $\mathbf{R}^{(2)}$, see Eq. (3) and Eq. (5), for the semi-discretization. The aforementioned spatial operators are discretized using DGSEM, which will be described in Sec. 3. Given the approximate solution $\mathbf{w}^n$ at time t^n, the s-stage diagonally implicit two-derivative SSP Runge-Kutta method can be written in Butcher form,

$$\mathbf{w}^{(i)} := \mathbf{w}^n + \Delta t \sum_{j=1}^{i} a_{ij} \mathbf{R}^{(1)}(\mathbf{w}^{(j)}) + \Delta t^2 \sum_{j=1}^{i} \dot{a}_{ij} \mathbf{R}^{(2)}(\mathbf{w}^{(j)}, \mathbf{R}^{(1)}(\mathbf{w}^{(j)})), \quad 1 \leq i \leq s. \tag{6}$$

The solution at time t^{n+1} is updated with

$$\mathbf{w}^{n+1} := \mathbf{w}^{(s)}. \tag{7}$$

The authors derived the diagonally implicit two-derivative SSP scheme in [7] for orders up to four; see Tab. 1. The Butcher coefficients $\mathbf{A} = \{a_{ij}\}$ and $\dot{\mathbf{A}} = \{\dot{a}_{ij}\}$ for the schemes can be found in [7, Sec. 2.3]. In Sec. 2.1, we analyze the linear stability of the implicit SSP schemes (Tab. 1).

Scheme	**Order**	**Stages**	A(α)-**Stability**
SSP-I2DRK21	2	1	A(90.00°)
SSP-I2DRK32	3	2	A(79.94°)
SSP-I2DRK45	4	5	A(84.52°)

Table 1: Strong stability preserving schemes from [7, Sec. 2.3]. The A(α) stability analysis can be found in Sec. 2.1 of the current paper.

2.1 Linear stability of the implicit two-derivative SSP schemes

In this section, the linear stability of the implicit two-derivative SSP method has been analyzed using Dahlquist's equation $w' = \lambda w$, where $\lambda \in \mathbb{C}$. We first derive the stability function for an s-stage SSP scheme, and then the linear stability for each of the schemes (see Tab. 1) will be analyzed in the following subsections. Plugging in $\mathbf{R}^{(1)} = \lambda w$ and $\mathbf{R}^{(2)} = \lambda w' = \lambda^2 w$ in Eq. (6) we get

$$w^{(i)} = y^n + \sum_{j=1}^{i} \left(a_{ij} \Delta t \lambda + \dot{a}_{ij} \Delta t^2 \lambda^2 \right) w^{(j)} \tag{8}$$

for each of the stages up to s. Define $z := \Delta t \lambda$ and functions $\mathcal{S}_i(z)$, so that the stage values $w^{(i)}$ in Eq. (8) can be explicitly written as

$$w^{(i)} = \mathcal{S}_i(z) w^n.$$

For $i \geq 2$, these functions can be recursively written as

$$\mathcal{S}_i(z) = \frac{1 + \sum_{j=1}^{i-1} \left(a_{ij} z + \dot{a}_{ij} z^2\right) \mathcal{S}_j(z)}{\left(1 - a_{ii} z - \dot{a}_{ii} z^2\right)} \text{ with } \mathcal{S}_1(z) = (1 - a_{11} z - \dot{a}_{11} z^2)^{-1}.$$

Then the update w^{n+1} can be written as

$$w^{n+1} = \mathcal{S}_s(z) w^n = \left(\frac{1 + \sum_{j=1}^{s-1} \left(a_{sj} z + \dot{a}_{sj} z^2\right) \mathcal{S}_j(z)}{\left(1 - a_{ss} z - \dot{a}_{ss} z^2\right)} \right) y^n =: \mathcal{S}(z) w^n, \tag{9}$$

where $\mathcal{S}(z)$ is the stability function.

Second-order SSP scheme

The second order SSP scheme SSP-I2DRK21 is none other than second-order Taylor method. From Eq. (9), the stability function for SSP-I2DRK21 is given by

$$\mathcal{S}(z) = \mathcal{S}_1(z) = \frac{2}{2 - 2z + z^2} \text{ for } z \in \mathbb{C}. \tag{10}$$

Then for the modulus value $|\mathcal{S}(z)|$

$$\max_{z \in \mathbb{C}^-} |\mathcal{S}(z)| \leq \max_{y \in \mathbb{R}} |\mathcal{S}(iy)| = \max_{y \in \mathbb{R}} \frac{2}{|(2 - y^2) - 2yi|} = \max_{y \in \mathbb{R}} \frac{2}{\sqrt{y^4 + 4}} \leq 1,$$

which implies that the second-order SSP method is **A-stable**, see [11, Chap. 5]. The method is also **L-stable** because,

$$\lim_{z \to \infty} \mathcal{S}(z) = 0.$$

Third-order SSP scheme

The stability function for SSP-I2DRK32 is given by

$$\mathcal{S}(z) = \mathcal{S}_2(z) = \frac{18}{(6 + z^2)(3 - 3z + z^2)} \text{ for } z \in \mathbb{C}. \tag{11}$$

It can be found from Eq. (11) that $\mathcal{S}(z)$ has singularities on the boundary of the domain $\mathbb{C}^-$ at $z = \pm i\sqrt{6}$. In Fig. 1 (a), the stability region ($|\mathcal{S}(z)| < 1$) has been plotted for the values $-5 \leq \text{Re}(z) \leq 5$ and $-6 \leq \text{Im}(z) \leq 6$. The stability region is represented by the areas shaded in blue in Fig. 1 (a). It can be seen that the stability region does not cover the entire negative complex half-plane, which implies that the method is **not A-stable**. Using the algorithm from [30, Sec. 3], it can be found that the method is approximately A(79.94°) stable.

Fourth-order SSP scheme

The stability function for SSP-I2DRK45 is given by

$$\mathcal{S}(z) = \mathcal{S}_5(z) = \frac{1 + \sum_{j=1}^{4} \left(a_{5j} z + \dot{a}_{5j} z^2\right) \mathcal{S}_j(z)}{\left(1 - a_{55} z - \dot{a}_{55} z^2\right)} \text{ for } z \in \mathbb{C} \tag{12}$$

with the Butcher coefficients given in [7, Sec. 2.3]. Similarly to the third order SSP scheme, the stability region (blue shaded region in Fig. 1 (b)) of the fourth order scheme also does not cover the entire negative complex half-plane, which implies that the method is **not A-stable**; the method is approximately A(84.52°) stable.

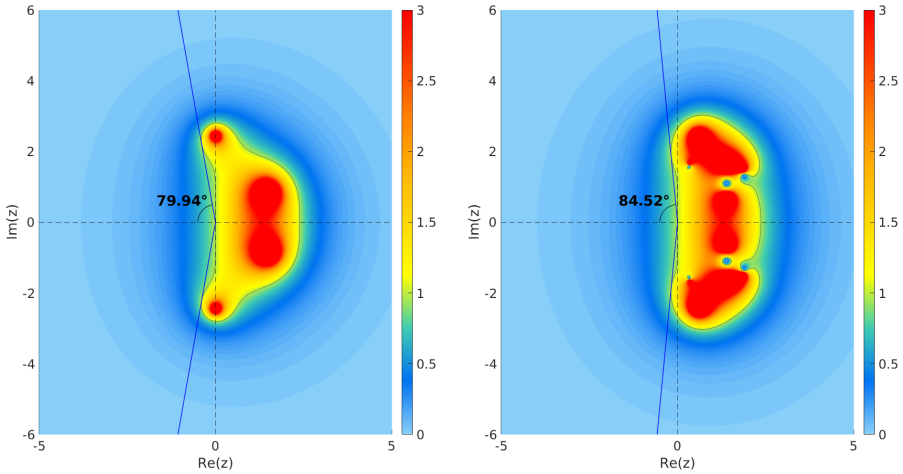

(a) SSP-I2DRK32 (b) SSP-I2DRK45

Figure 1: Stability region ($|\mathcal{S}(z)| < 1$) for third order (a) and fourth order (b) SSP schemes. Stability angle is found using the algorithm from [30, Sec. 3] via the stability functions given in Eq. (11) and Eq. (12) respectively.

2.2 Non-existence of an A-stable implicit two-derivative two-stage third-order SSP scheme

As the SSP-I2DRK32 scheme exhibits a relatively low stability angle, we develop an improved scheme in this section.

Lemma 1. *There is no diagonally implicit two-derivative two-stage third-order scheme which is both* ***A-stable*** *and* ***SSP*** *according to the conditions in [7, Theorem 1].*

Proof. We utilize the order conditions for third-order accuracy from [7, Sec. 2.1] along with the SSP conditions from [7, Sec. 2.2] and [7, Theorem 1] to derive the Butcher coefficients

$$\mathbf{A} = \begin{bmatrix} \rho & 0 \\ \phi & \eta \end{bmatrix} \text{ and } \dot{\mathbf{A}} = \begin{bmatrix} \alpha & 0 \\ \gamma & \beta \end{bmatrix}. \tag{13}$$

So, for $0 < k \leq 1$ we have

$$\phi = k\rho \text{ and } \gamma = k\alpha \tag{14}$$

where $\rho \geq 0$, $\eta \geq 0$, $\alpha \leq 0$ and $\beta \leq 0$. Now, rewrite the Butcher coefficients (13) with the aforementioned SSP conditions and the first-order condition ($\phi + \eta = 1$) to obtain

$$\mathbf{A} = \begin{bmatrix} \rho & 0 \\ k\rho & 1 - k\rho \end{bmatrix} \text{ and } \dot{\mathbf{A}} = \begin{bmatrix} \alpha & 0 \\ k\alpha & \beta \end{bmatrix}. \tag{15}$$

Now, applying the second-order condition [7, Sec. 2.1, $p = 2$] we get

$$\beta = k(\rho - \rho^2 - \alpha) - \frac{1}{2}. \tag{16}$$

Consider Eq. (16) and apply the third-order conditions [7, Sec. 2.1, $p = 3$] to obtain

$$k(\rho^3 - 2\rho^2 + 2\rho\alpha + \rho - 2\alpha) = \frac{1}{3}, \tag{17}$$

$$k(2\rho^3 - 2\rho^2 + 4\rho\alpha + \rho - 2\alpha) = \frac{1}{3}. \tag{18}$$

We assume that $k \neq 0$ because the third order conditions (see [7, Sec. 2.1]) give rise to an inconsistent system of equations for $k = 0$ (see Eqs. (17) and (18)). Now, we can solve the equations (17) and (18) for ρ by eliminating k. Hence we have

$$\rho^3 + 2\alpha\rho = 0 \;\Rightarrow\; \rho = 0, \text{ or } \rho = \pm\sqrt{-2\alpha}.$$

We start with the non-zero solution. From the condition that $\alpha \leq 0$, take $\alpha = -2\mu^2$, for $\mu > 0$. Since the SSP property [7, Theorem 1] necessitates a non-negative ρ, the non-zero solution is

$$\rho = 2\mu, \;\; \mu > 0. \tag{19}$$

Substituting for α and ρ in (17) or (18) gives

$$k = \frac{1}{6(\mu - 2\mu^2)}, \;\; \mu > 0. \tag{20}$$

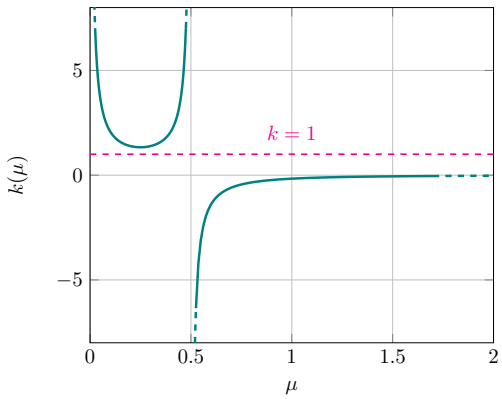

Figure 2: Graph of variable k (20) from the Butcher coefficients (15), obtained as a function of μ using the order equations (17) and (18). The function $k(\mu) = \frac{1}{6(\mu - 2\mu^2)}$ never reaches values from (0,1] for any values of $\mu > 0$.

The values of k have been plotted in Fig. 2 for $\mu > 0$. It can been seen clearly from Fig. 2 that

$$k = \begin{cases} > 1, \;\; 0 < \mu < 0.5 \\ < 0, \;\; \mu > 0.5 \end{cases}. \tag{21}$$

So, there are no values for $\mu > 0$ such that $0 < k \leq 1$. Now consider the case when $\rho = 0$. Then from Eq. (17) and Eq. (16) we get

$$k\alpha = -\frac{1}{6}, \text{ and } \beta = -\frac{1}{3}. \tag{22}$$

Hence there are infinitely many possibilities for third-order SSP schemes when $\rho = 0$ and it is given by

$$\mathbf{A} = \begin{bmatrix} 0 & 0 \\ 0 & 1 \end{bmatrix} \text{ and } \dot{\mathbf{A}} = \begin{bmatrix} -\frac{1}{6k} & 0 \\ -\frac{1}{6} & -\frac{1}{3} \end{bmatrix}, \ 0 < k \leq 1. \tag{23}$$

The SSP scheme (23) is the same third-order SSP scheme referred to in [7] for $k = 1$. The stability function for the scheme (23) is

$$\mathcal{S}(z) = \frac{18k + 3(1-k)z^2}{(6k + z^2)(3 - 3z + z^2)}, \tag{24}$$

and the scheme (23) can **never be A-stable** as $\mathcal{S}(z)$ has singularities at $\pm i\sqrt{6k}$. □

2.3 A family of A(α)-stable implicit two-derivative two-stage third-order SSP scheme

Even though the third-order SSP scheme discussed above cannot be A-stable, the analysis in the previous section has led to a family of A(α)-stable implicit two-derivative, two-stage, third-order SSP schemes, as given in (23), parameterized by a free variable k. The α angles are plotted against different k values in Fig. 3. It can be noted from Fig. 3 that the schemes (23) are tending towards $A(90^o)$ as $k \to 0$. However, the Butcher coefficient $\dot{a}_{11} = -\frac{1}{6k} \to -\infty$, which can significantly affect the error constant of the schemes.

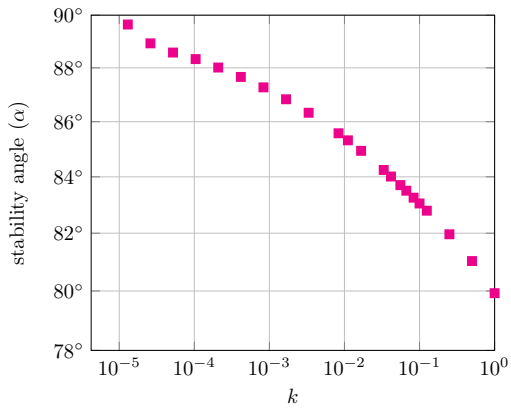

Figure 3: Stability angles α for the $A(\alpha)$-stable two-derivative two-stage third-order scheme (23) are plotted for different values of the free variable $0 < k \leq 1$.

Consider the stability regions plotted in Fig. 4 to analyze the effect of the free parameter k on the stability angle. It can be seen in Fig. 4 that, as $k \to 0$, the poles on the imaginary axis ($\pm i\sqrt{6k}$) move toward the origin. Meanwhile, the unstable region in the left half of the complex plane becomes smaller, resulting in an increase in the stability angle. This poses a significant issue because, as Δt approaches 0, the term $z = \Delta t\, \lambda$ tends to concentrate around the origin, where λ represents the eigenvalues of the discretized ODE system.

In the upcoming sections, the family of $A(\alpha)$ stable third-order SSP schemes (23) with $0 < k < 1$, will be denoted as SSP-I2DRK32(k). When $k = 1$, SSP-I2DRK32(1) refers to the original scheme SSP-I2DRK32. For values of $k > 1$, the schemes are no longer SSP, and we will denote them as NSSP-I2DRK32(k).

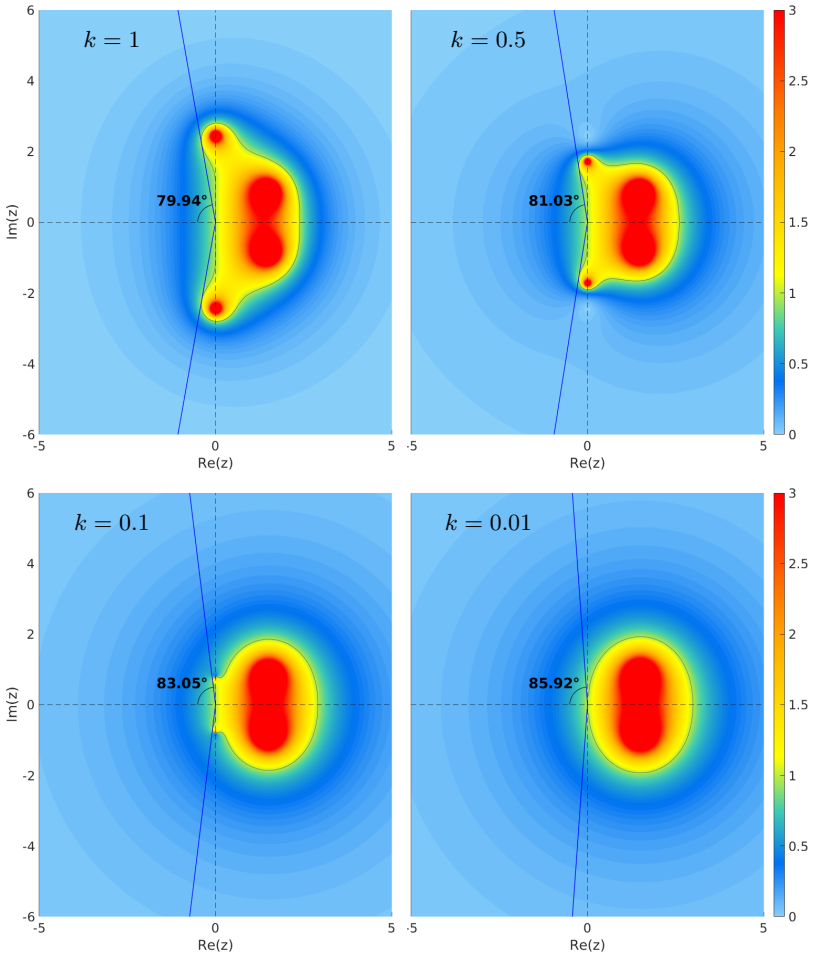

Figure 4: Stability region ($|\mathcal{S}(z)| < 1$) for the third-order SSP scheme SSP-I2DRK32(k), plotted using the algorithm from [30, Sec. 3] via the stability functions in Eq. (24) for different values of the free parameter k.

3 Fully discrete formulation

We use the discontinuous Galerkin spectral element method which has been introduced in [17] for the spatial discretization. The spatial domain Ω under consideration is subdivided into $\mathrm{N_E}$ quadrangular (2D) or hexahedral (3D) elements Ω_e. The discrete formulation of the DGSEM is recalled briefly in the following section by closely following the papers [31, 13]. The weak formulations for the first and second derivatives are provided only for the Euler equations in the following subsection; detailed formulations for the Navier–Stokes equations can be found in [31, Sec. 5].

3.1 Evaluation of the temporal derivatives with the DGSEM

The DGSEM utilizes the weak formulation of Eq. (1),

$$\sum_{e=1}^{\mathrm{N_E}}(\mathbf{w}_t,\phi)_{\Omega_e}-(\mathbf{F}(\mathbf{w}),\nabla\phi)_{\Omega_e}+\left\langle\mathbf{F}^*(\mathbf{w}^L,\mathbf{w}^R)\cdot\mathbf{n},\phi\right\rangle_{\partial\Omega_e}=0,\ \forall\phi\in\Pi_{\mathrm{N_p}},\tag{25}$$

where $\Pi_{\mathrm{N_p}}$ is the space of test functions constructed by the tensor product of the one-dimensional Lagrange interpolation polynomials of degree $\mathrm{N_p}$. The scalar product $(\cdot,\cdot)_{\Omega_e}$ denotes the element-wise integration over the elements Ω_e and $\langle\cdot,\cdot\rangle_{\partial\Omega_e}$ is the integration along the cell-edges $\partial\Omega_e$. The flux function is replaced by a numerical flux function $F^*(\mathbf{w}^L,\mathbf{w}^R)$ on the cell-edges, which depends on the left and right states with respect to the cell-edge, and $\mathbf{n}$ is the outward pointing normal to the cell-edge. The global Lax-Friedrichs flux is used as the numerical flux (see [31, Eq. (13) and Eq. (17)]). The spatial DGSEM operator for the first time derivative $\mathbf{R}_h^{(1)}(\mathbf{w}_h)$ is given in [31, Eq. (12)].

As we use two-derivative time stepping schemes (6), it is required to compute the spatial DGSEM operator for the second derivative. The spatial operator for the second derivative is evaluated by introducing the artificial quantity

$$\boldsymbol{\sigma}:=\mathbf{R}^{(1)}(\mathbf{w})\equiv\mathbf{w}_t\tag{26}$$

as done in [26]. Differentiating Eq. (25) with respect to time and applying $\boldsymbol{\sigma}$, we get,

$$\sum_{e=1}^{\mathrm{N_E}}(\mathbf{w}_{tt},\phi)_{\Omega_e}-\left(\frac{\partial\mathbf{F}(\mathbf{w})}{\partial\mathbf{w}}\boldsymbol{\sigma},\nabla\phi\right)_{\Omega_e}+\left\langle\frac{\partial\mathbf{F}^*(\mathbf{w}^L,\mathbf{w}^R)}{\partial\mathbf{w}^L}\boldsymbol{\sigma}^L\cdot\mathbf{n}+\frac{\partial\mathbf{F}^*(\mathbf{w}^L,\mathbf{w}^R)}{\partial\mathbf{w}^R}\boldsymbol{\sigma}^R\cdot\mathbf{n},\phi\right\rangle_{\partial\Omega_e}=0,\forall\phi\in\Pi_{\mathrm{N_p}}.\tag{27}$$

The spatial DGSEM operator for the second time derivative $\mathbf{R}_h^{(2)}(\mathbf{w}_h,\mathbf{R}^{(1)})$ is also evaluated similarly to that of the first time derivative and it is given in [31, Eq. (16)].

The SSP schemes [7] for the conservation laws (1) are implemented in the open source code FLEXI[1], which was developed for solving hyperbolic-parabolic conservation equations in a discontinuous Galerkin setting [18].

3.2 Preconditioning of the extended linear system

The stage values in Eq. (6) can be solved using Newton's method. For the i^{th} stage, the equation can be cast into the non-linear form

$$\mathbf{G}(\mathbf{w}^{(i)}):=\mathbf{g}(\mathbf{w}^{(i)})-\mathbf{b}=0,\tag{28}$$

where the function $\mathbf{g}$ and vector $\mathbf{b}$ are given by

$$\begin{aligned}\mathbf{g}(\mathbf{w}^{(i)})&=\mathbf{w}^{(i)}-\Delta t a_{ii}\mathbf{R}^{(1)}(\mathbf{w}^{(i)})-\Delta t^2\dot{a}_{ii}\mathbf{R}^{(2)}(\mathbf{w}^{(i)},\mathbf{R}^{(1)}(\mathbf{w}^{(i)})),\\ \mathbf{b}&=\mathbf{w}^n+\Delta t\sum_{j=1}^{i-1}a_{ij}\mathbf{R}^{(1)}(\mathbf{w}^{(j)})+\Delta t^2\sum_{j=1}^{i-1}\dot{a}_{ij}\mathbf{R}^{(2)}(\mathbf{w}^{(j)},\mathbf{R}^{(1)}(\mathbf{w}^{(j)})).\end{aligned}$$

More details over the non-linear formulation (28) can be found in [31, Sec. 3.2.1]. The linear system which arises in every Newton step is solved using the GMRES method. For faster convergence of the GMRES, application of a preconditioner is necessary.

[1] http://www.flexi-project.org

In [31, Sec. 4], the authors have compared the effect of different preconditioners on linear and non-linear iterations (see [31, Fig. 2 and Fig. 4]) and found that problem-tailored extended Block-Jacobi preconditioners $\mathbf{BJ^H_{ext}}$ and $\mathbf{BJ_{ext}}$ perform better than standard Block-Jacobi and ILU(0) preconditioners, in terms of the GMRES iterations per timestep and the wall-clock time. Consult [31, Fig. 1] for the pictorial representation of the mentioned precondition matrices. The authors employed a matrix-free approach with the $\mathbf{BJ_{ext}}$ preconditioner for their numerical investigations in [31], as it was efficient and effective. See the papers [6] and [16] for the matrix-free implementation. In this paper, we also use the matrix free approach with $\mathbf{BJ_{ext}}$ preconditioning as implemented in [31, Sec. 4.2].

4 Numerical investigations

As discussed in the previous section, we use Newton's method for solving the implicit equations and employ GMRES to solve the linear equations that arise in each Newton step. For a given Newton tolerance $\varepsilon_{\text{Newton}}$, the stopping criterion for the k^{th} Newton iteration is given by

$$\left\|\mathbf{G}(\mathbf{X}^k)\right\| < \varepsilon_{\text{Newton}} \cdot \left\|\mathbf{G}(\mathbf{X}^0)\right\|,$$

where $\left\|\mathbf{G}(\mathbf{X}^k)\right\|$ and $\left\|\mathbf{G}(\mathbf{X}^0)\right\|$ are the L_2 norms of the k^{th} and initial residuals, respectively. For a specified tolerance for the linear solver, $\varepsilon_{\text{GMRES}}$, the stopping criterion for the GMRES iterations for the k^{th} Newton increment is

$$\left\|\mathbf{r}^k\right\| < \varepsilon_{\text{GMRES}} \cdot \left\|\mathbf{G}(\mathbf{X}^{k-1})\right\|,$$

where $\mathbf{r}^k$ is the residual of the linear equation, as indicated in [31, Eq. 18]. Test cases are described in the following sections.

4.1 Linear advection equation

Consider the two-dimensional linear advection equation

$$\mathbf{w}_t + \nabla \cdot (\mathbf{a}\mathbf{w}) = 0, \tag{29}$$

where $\mathbf{a} \in \mathbb{R}^2$ is a constant vector. We consider an exact solution of the equation (29) given by

$$\mathbf{w}(x,t) = \sin\left(\pi \sum_{j=1}^{2} (x_j - a_j t)\right), \tag{30}$$

with $\mathbf{a} = (0.3, 0.3)$ and $x \in \Omega = [-1,1]^2$ with periodic boundary conditions to analyze the SSP schemes. The classic upwind flux is chosen as the numerical flux for the DGSEM spatial discretization.

The L_2-error, average Newton iterations per timestep per stage and average GMRES iterations per Newton iteration for linear advection of a sine wave with $T_{\text{end}} = 0.8$ and $T_{\text{end}} = 1.6$ are presented in Fig. 5. The plots in Fig. 5 show that both the second-order and fourth-order SSP schemes exhibit the expected convergence for all the timestep sizes considered for $T_{\text{end}} = 0.8$ and $T_{\text{end}} = 1.6$. However, the third-order scheme encounters convergence issues for certain timesteps and requires greater number of Newton and GMRES iterations compared to the second and fourth-order schemes. Additionally, the severity of divergence in the third-order SSP scheme increases for the larger final time of $T_{\text{end}} = 1.6$.

A comprehensive study on the third-order SSP scheme is presented in Sec. 4.1.1 using the linear advection equation discretized using DGSEM. Additionally, a few strategies are discussed in Sec. 4.1.2 to control the divergence of the algorithm.

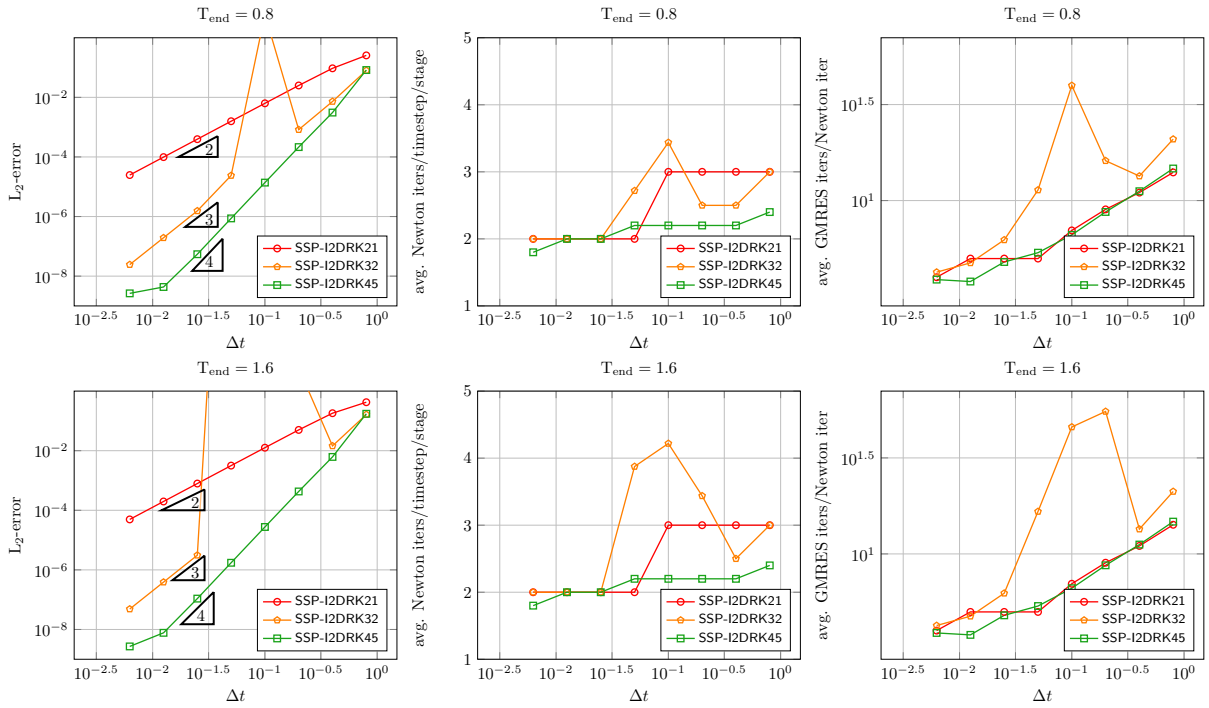

Figure 5: L_2-error (left), average Newton iterations per timestep per stage (middle) and average GMRES iterations per Newton iteration (right) for linear advection of a sine wave with $T_{end} = 0.8$ (top) and $T_{end} = 1.6$ (bottom). The initial condition is evaluated from (30) and simulated using the SSP schemes for different timesteps Δt. The spatial discretization is set to $N_E = 16 \times 16$ and $N_p = 5$. A tolerance of $\varepsilon_{Newton} = 10^{-6}$ and $\varepsilon_{GMRES} = 10^{-3}$ is used, with a limit of 10 Newton iterations per implicit solve and 2000 GMRES iterations per Newton iteration.

4.1.1 Analysis of the constraints in the third-order SSP scheme

As discussed in the previous section, the third-order SSP scheme exhibits convergence issues over a specific range of timestep sizes when applied to the linear advection of a sine wave. The initial condition was evaluated using equation (30), and the DGSEM spatial discretization was configured with $N_E = 16 \times 16$ elements and polynomial degree $N_p = 5$. To investigate the influence of the stability angle on the under-performance of the SSP-I2DRK32 scheme, we first consider a two-derivative, diagonally implicit, third-order Runge-Kutta scheme (I2DRK32(79.94°)), which possesses the same stability angle (79.94°) as the SSP-I2DRK32 scheme. The construction of the I2DRK32(79.94°) (44) is given in A.1.

In Fig. 6, we compare the convergence, average Newton and GMRES iterations required for implicit solves using the SSP-I2DRK32 scheme and the I2DRK32(79.94°) scheme. The results indicate that although the I2DRK32(79.94°) scheme has the same stability angle as the SSP-I2DRK32, it achieves the desired error reduction with a similar Newton and GMRES consumption as the second and fourth-order SSP schemes (see Fig. 5). Therefore, as a preliminary conclusion from Fig. 6, it is not the stability angle that affects the convergence of the SSP-I2DRK32 scheme. Hence, a detailed investigation on the stability regions is necessary.

The stability regions for the SSP-I2DRK32 and I2DRK32(79.94°) schemes are illustrated in Fig. 7. Although

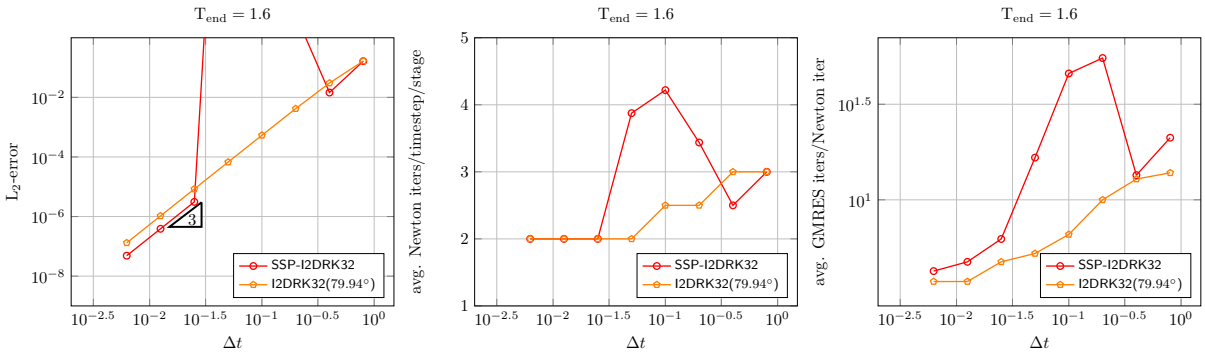

Figure 6: L_2-error (left), average Newton iterations per timestep per stage (middle) and average GMRES iterations per Newton iteration (right) for linear advection of a sine wave with $T_{end} = 1.6$. The initial condition is evaluated from (30). The spatial discretization is set to $N_E = 16 \times 16$ and $N_p = 5$. A tolerance of $\varepsilon_{\text{Newton}} = 10^{-6}$ and $\varepsilon_{\text{GMRES}} = 10^{-3}$ is used, with a limit of 10 Newton iterations per implicit solve and 2000 GMRES iterations per Newton iteration.

both schemes have the same stability angle of 79.94°, the locations of their unstable regions near the imaginary axis, which determine the stability angle, differ. To understand the influence of differences in unstable regions, we need

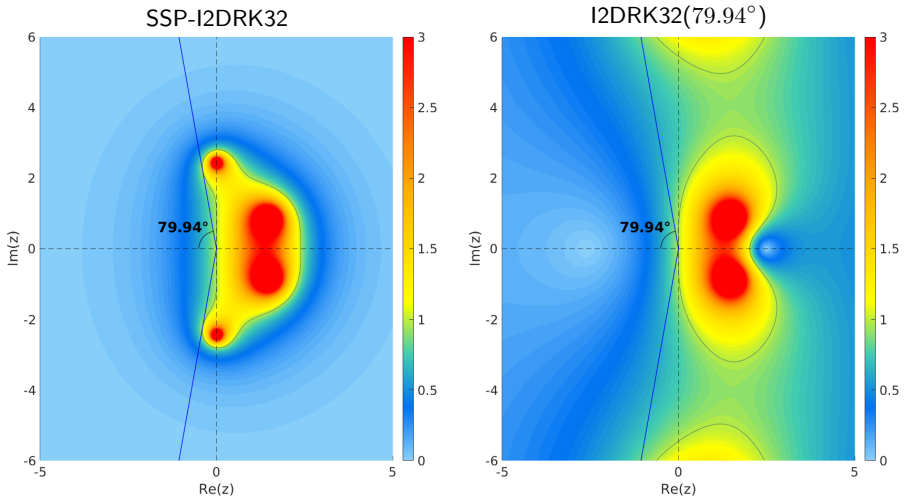

Figure 7: Stability region ($|\mathcal{S}(z)| < 1$) for SSP-I2DRK32 scheme (left) and I2DRK32(79.94°) scheme (right).

to examine the eigenvalues of the Jacobian of the spatially discretized part, $-\nabla \cdot \mathbf{F}$, from Eq. (1). Let Λ be the set of eigenvalues corresponding to the linear advection equation in Sec. 4.1.1 with discretization set to $N_E = 16 \times 16$ and $N_p = 5$. Note that for linear advection equations, the Jacobian corresponding to the spatially discretized ODE system is a constant matrix.

From Fig. 6, it can be observed that the range of timestep sizes that experience convergence issues is $\Delta t =$

$\{0.2, 0.1, 0.05\}$. Therefore, in Fig. 8 we plot the points

$$\mathbf{Z} = \Delta t \Lambda,$$

on the stability regions for both the SSP-I2DRK32 and I2DRK32(79.94°) schemes. It is clear that the values of $\mathbf{Z}$ fall into the unstable regions for all timestep sizes $\Delta t = \{0.2, 0.1, 0.05\}$ for the SSP-I2DRK32 scheme. Thus, the stability function (Eq. 11) generates values greater than one for the components associated with eigenvalues that are in the unstable regions. As the number of timesteps varies between 8 and 32, the error accumulates over these timesteps, leading to diverging solutions. The increase in the number of Newton and GMRES iterations observed in Figs. 5 and 7 might have resulted from several factors: error accumulation due to stability, a poor initial guess for the Newton method—since we used previous stage solutions as the initial guess—and higher residual norms, see Eq. (28).

In the case of the I2DRK32(79.94°) scheme, almost all values of $\mathbf{Z}$ fall into stable regimes for timestep sizes $\Delta t = \{0.1, 0.05\}$, and therefore, the desired convergence is achieved. Although a few eigenvalues fall into the unstable region for $\Delta t = 0.2$, the lower severity of the stability function ($|\mathcal{S}(z)| \lesssim 4$) and the reduced number of time steps help minimize error accumulation. In comparison, the absolute stability function ($|\mathcal{S}(z)|$) reaches values up to 40 in the unstable regimes for the SSP-I2DRK32 scheme.

Therefore, from the Figs. 7 and 8, it can be concluded that it is not the stability angle, but *the position of the unstable region near the imaginary axis* that contributes to the convergence issues for the SSP-I2DRK32 scheme.

4.1.2 A k-adaptive SSP scheme

As discussed in the previous section, the occurrence of values $\Delta t\Lambda$ in the unstable region leads to error accumulation, resulting in a solution divergence when using the SSP-I2DRK32 scheme. Fig. 9 shows that a convergent solution for a specified timestep Δt can be achieved by selecting an appropriate SSP-I2DRK32(k) or NSSP-I2DRK32(k) scheme. However, not all values of k yield convergent solutions. Therefore, we aim to explore the relationship between Δt and the free parameter k to develop a k-adaptive scheme, referred to as AD-SSP-I2DRK32 for the adaptive SSP scheme and AD-NSSP-I2DRK32 for the adaptive non-SSP scheme.

In [19], the authors analyzed the one-dimensional linear advection equation using a discontinuous Galerkin spatial discretization with upwinding and periodic boundary conditions. They found that the eigenvalues Λ of the discretization matrix can be bounded by a value that depends on the wave speed $a \in \mathbb{R}$, the spatial mesh size Δx, and the polynomial degree $\mathrm{N_p}$. They proved that the growth rate of the largest eigenvalues is less than $(\mathrm{N_p}+1)^2$, and more precisely, they conjectured that it is proportional to $(\mathrm{N_p}+1)^{1.75}$.

Taking into account the eigenvalue bounds described in [19], we modifiy it slightly for the two-dimensional linear advection equation (29), with wave velocity $\mathbf{a} \in \mathbb{R}^2$. Hence, we consider a bound on maximum absolute value of the eigenvalue given by

$$\Lambda_{\max} := \frac{\sum |\mathbf{a}_i|}{\Delta x}(\mathrm{N_p}+1)^{1.75}. \tag{31}$$

As seen in Sec. 2.2, the stability of the family of third-order schemes (24) has poles at $\pm\sqrt{6k}i$. Therefore by analyzing the distribution eigenvalues in Fig. 8, we consider the following assumption

$$\sqrt{6k} \geq \Delta t \Lambda_{\max} \tag{32}$$

to make sure that no values $\Delta t\Lambda$ is falling on the unstable region of the schemes (23). From Eq.(32), we derive

$$k_{\min} := \frac{(\Delta t \Lambda_{\max})^2}{6} \tag{33}$$

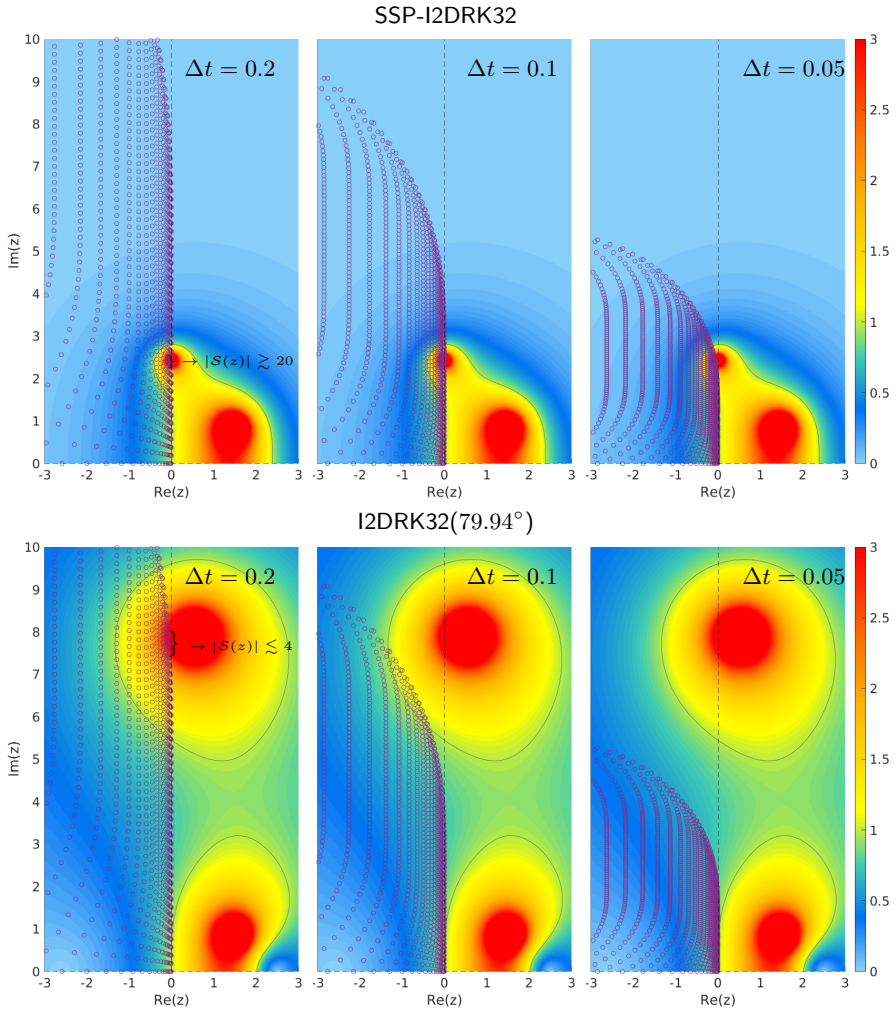

Figure 8: The stability regions for the SSP-I2DRK32 scheme and the I2DRK32(79.94°) scheme are given in the top and bottom rows, respectively. The values $\mathbf{Z} = \Delta t\Lambda$ are plotted (purple circles) for the eigenvalues Λ corresponding to the linear advection equation discussed in Sec. 4.1.1, with the discretization set to $\mathrm{N_E} = 16 \times 16$ and $\mathrm{N_p} = 5$. The points $\mathbf{Z} = \Delta t\Lambda$ are plotted for timestep sizes $\Delta t = \{0.2, 0.1, 0.05\}$. The real and imaginary axes are restricted to the ranges $-3 \leq \mathrm{Re}(z) \leq 3$ and $0 \leq \mathrm{Im}(z) \leq 10$.

which is the minimum k value needed for the scheme (23) so as to assure a converging solution for a given Δt. Hence the non-SSP adaptive scheme is given by

$$\text{AD-NSSP-I2DRK32} := \begin{cases} \text{SSP-I2DRK32}, & \Delta t\Lambda_{\max} \leq \sqrt{6} \\ \text{NSSP-I2DRK32}(k_{\min}), & \text{otherwise} \end{cases} . \tag{34}$$

Since the non-SSP does not guarantee $k_{\min} \leq 1$ for every Δt, we need a slightly different approach to develop an

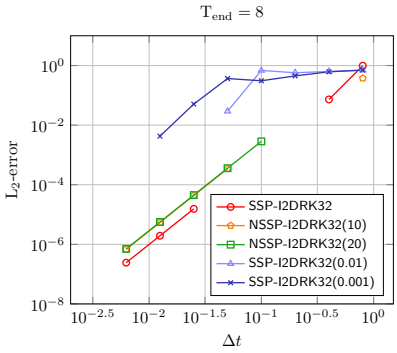

Figure 9: L_2-error for linear advection of a sine wave with $T_{end} = 8$ using various third-order schemes. The initial condition is evaluated from (30). The spatial discretization is set to $N_E = 16 \times 16$ and $N_p = 5$. A tolerance of $\varepsilon_{Newton} = 10^{-6}$ and $\varepsilon_{GMRES} = 10^{-3}$ is used, with a limit of 20 Newton iterations per implicit solve and 2000 GMRES iterations per Newton iteration. Note that the missing points on the plots indicate diverged solutions.

adaptive SSP scheme. Consider the absolute value of stability function for SSP-I2DRK32(k) along the imaginary axis

$$\begin{aligned} |\mathcal{S}(iy)| &= \left| \frac{18k + 3(1-k)(iy)^2}{(6k + (iy)^2)(3 - 3(iy) + (iy)^2)} \right|, \\ &= \left| \frac{18k + 3(k-1)y^2}{(6k - y^2)} \right| \frac{1}{\sqrt{y^4 + 3y^2 + 9}}. \end{aligned}$$

To find the points where the absolute value equals one on the imaginary axis, we set $|\mathcal{S}(iy)|^2$ to one, which yields

$$y^4 \left(y^4 + (3 - 12k)\, y^2 + \left(27k^2 - 18k\right) \right) = 0.$$

Analyzing the roots of this equation, we find that the real roots lie in the interval

$$\mathbf{I} := \left[-\sqrt{6k + \frac{3}{2}\left(\sqrt{4k^2+1} - 1\right)}, \sqrt{6k + \frac{3}{2}\left(\sqrt{4k^2+1} - 1\right)} \right].$$

For visual clarity, refer to the stability regions shown in Fig. 4. Let $l_\Lambda > 0$ be a value slightly less than the minimum modulus of eigenvalues in Λ that have a non-zero imaginary part and a real part very close to zero. For a clearer visual understanding of l_Λ, refer to Fig. 10. Therefore, to achieve a stable SSP solution for a given time step Δt, we require

$$\sqrt{6k + \frac{3}{2}\left(\sqrt{4k^2+1} - 1\right)} = \Delta t l_\Lambda. \tag{35}$$

The condition (35) ensures that the set $\mathbf{I}$ is contained within the interval $[-\Delta t l_\Lambda, \Delta t l_\Lambda]$. Consequently, this implies that there are no eigenvalues present in the unstable region. Hence, the stable SSP adaptive scheme is given by

$$\text{AD-SSP-I2DRK32} := \begin{cases} \text{SSP-I2DRK32}, & \Delta t \Lambda_{max} \leq \sqrt{6} \\ \text{SSP-I2DRK32}(k_{\text{small}}), & \text{otherwise} \end{cases} \tag{36}$$

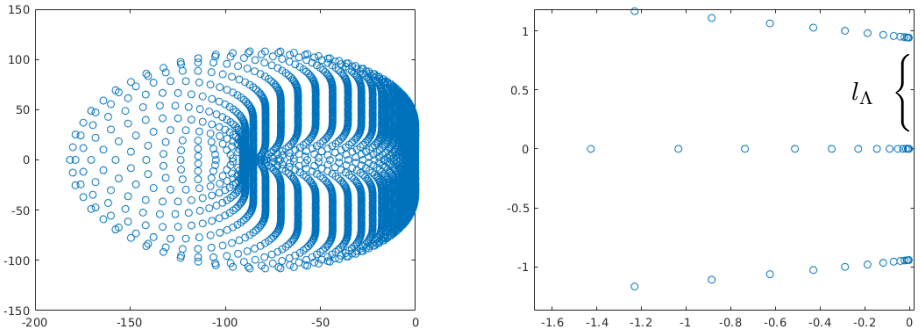

Figure 10: The eigenvalues Λ (shown on the left) corresponding to the linear advection equation discussed in Sec. 4.1.1, with a discretization set to $\mathrm{N_E} = 16 \times 16$ and $\mathrm{N_p} = 5$. On the right, a zoomed-in plot of the eigenvalues Λ is provided, with l_Λ marked on it.

with $k_{\text{small}} := \min(k_{\Delta t}, 1)$, where $k_{\Delta t}$ is the root of the equation defined above. Note that the value l_Λ must be known a priori. For the linear advection equation (29) with $\mathbf{a} = (0.3, 0.3)$, discretized using $\mathrm{N_E} = 16 \times 16$ and $\mathrm{N_p} = 5$, the value l_Λ is found to be less than 0.9, See Fig. 10. In a different spatial discretization setting, l_Λ can only be determined by analyzing the distribution of the eigenvalues, which is a current limitation. Further study and analysis are needed to find an empirical formulation for l_Λ, which is beyond the scope of the current paper.

In Fig. 11, the convergence plots for the linear advection equation are presented for the SSP-I2DRK32, AD-NSSP-I2DRK32 and AD-SSP-I2DRK32 schemes, using various final times $\mathrm{T_{end}}$. It is evident that the AD-NSSP-I2DRK32 and AD-SSP-I2DRK32 schemes provide stable solutions for all given timestep sizes Δt, while the SSP-I2DRK32 scheme diverges for the majority of timestep sizes. The adaptive schemes maintain stability across all final times, $\mathrm{T_{end}} = 8, 16, 32$. The AD-NSSP-I2DRK32 scheme exhibits the desired convergence order for all timestep sizes. Although the AD-SSP-I2DRK32 scheme yields stable solutions, there is a noticeable degradation in order for several timestep sizes. The error constant for the SSP-I2DRK32(k) scheme is given by

$$\left| \frac{1}{36k} - \frac{1}{24} \right|.$$

Thus, smaller values of k result in larger error constants, which lead to order reductions.

4.2 Euler equations

We consider the two dimensional Euler equations of gas dynamics

$$\mathbf{w}_t + \nabla \cdot \mathbf{F}^{\text{inv}}(\mathbf{w}) = 0, \tag{37}$$

with the state vector $\mathbf{w} = \begin{pmatrix} \rho \\ \rho \mathbf{v} \\ E \end{pmatrix}$. The flux function $\mathbf{F}^{\text{inv}}$ is given by

$$\mathbf{F}^{\text{inv}}(\mathbf{w}) = \begin{pmatrix} \rho \mathbf{v} \\ \rho \mathbf{v} \otimes \mathbf{v} + p \cdot \mathbf{Id} \\ \mathbf{v}(E + p) \end{pmatrix}, \tag{38}$$

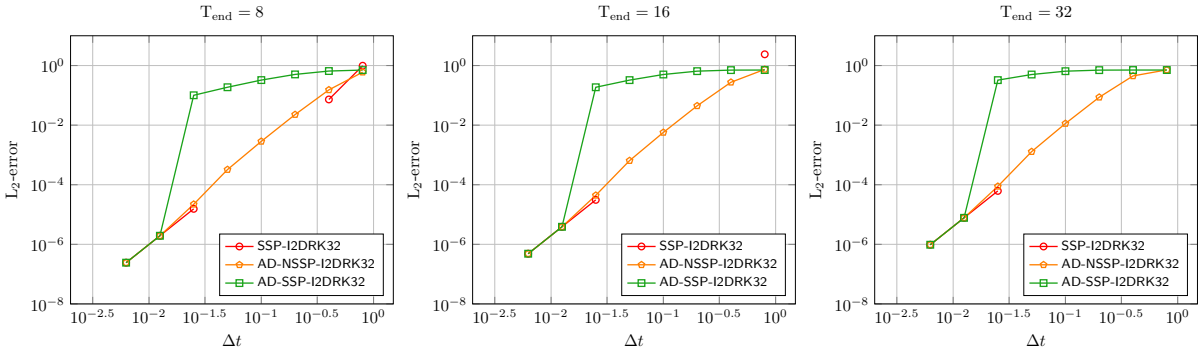

Figure 11: L_2-error for linear advection of a sine wave with $T_{end} = 8$ (left), $T_{end} = 16$ (middle) and $T_{end} = 8$ (right) using SSP-I2DRK32, AD-NSSP-I2DRK32 and AD-SSP-I2DRK32 schemes. The initial condition is evaluated from (30). The spatial discretization is set to $N_E = 16 \times 16$ and $N_p = 5$. A tolerance of $\varepsilon_{\text{Newton}} = 10^{-6}$ and $\varepsilon_{\text{GMRES}} = 10^{-3}$ is used, with a limit of 20 Newton iterations per implicit solve and 2000 GMRES iterations per Newton iteration. Note that the missing points on the plots indicate diverged solutions.

where ρ is density, $\mathbf{v} = (v_1, v_2)$ is velocity, E is total energy and p is pressure. Pressure is evaluated using the equation of state of a perfect gas,

$$p = (\gamma - 1)\Big(E - \frac{\rho}{2}\|\mathbf{v}\|_2^2\Big)$$

with the isentropic coefficient $\gamma = 1.4$. For the numerical validation of the Euler equations (37), we consider an extension of the linear advection equation (29) with a constant velocity $\mathbf{v} \equiv \mathbf{a} = (0.3, 0.3)^T$ and pressure $p = 1$. The initial conditions are therefore evaluated from the exact solution

$$\rho(x,t) = 1 + 0.3\sin\Big(\pi\sum_{j=1}^{2}(x_j - a_j t)\Big),\ \mathbf{v} = \mathbf{a},\ p = 1,\ x \in \Omega = [-1,1]^2, \tag{39}$$

and boundary conditions are taken to be periodic. The λ value for the global Lax-Friedrichs numerical flux (see [31, Eqs. (13) and (17)]) is chosen to be $\lambda = (1,1,1,1)$, as per the values given in [15].

The exact solution given in equation (39) serves as the reference solution for analyzing the L_2-error. The convergence results for the SSP-I2DRK21, SSP-I2DRK32, and SSP-I2DRK45 schemes are visualized in Fig. 12. For the SSP-I2DRK21 and SSP-I2DRK45 schemes, the errors decrease as the time step decreases, exhibiting the expected order of convergence. However, the SSP-I2DRK32 scheme diverges for $\Delta t \leq 0.2$. For the converged solutions, the number of Newton and GMRES iterations per implicit solve remains more or less the same.

In Fig. 13, we have presented the convergence plots, as well as the average Newton and GMRES iterations required for implicit solves, for the SSP-I2DRK32, AD-NSSP-I2DRK32 , and AD-SSP-I2DRK32 schemes. In contrast to the linear advection equations, the Euler equations have variable wave speeds given by $\{\mathbf{u}\cdot\mathbf{n}, \mathbf{u}\cdot\mathbf{n} \pm c\}$, where c is the speed of sound, defined as $c = \sqrt{\frac{\gamma p}{\rho}}$. As we consider Euler equations corresponding to the explicit solution (39), we can obtain an upper bound on the wave speeds in any direction $\mathbf{n}$. The upper bound is given by

$$\max\{\mathbf{u}\cdot\mathbf{n}, \mathbf{u}\cdot\mathbf{n} \pm c\} \leq |\mathbf{u}\cdot\mathbf{n}| + \sqrt{\frac{\gamma p}{\rho}} \leq 0.3 + \sqrt{\frac{1.4}{\min\rho}} = 0.3 + \sqrt{2}.$$

Consequently, we can evaluate $k_{\min}$ using the relation (31), replacing $\sum|\mathbf{a}_i| = 2(0.3+\sqrt{2})$. The AD-NSSP-I2DRK32 shows desired convergence order for all the timestep sizes, with relatively few GMRES iterations compared to

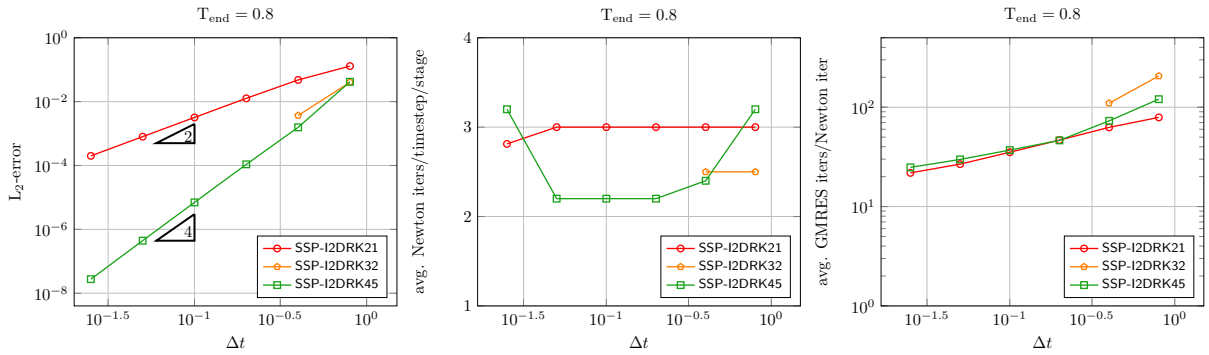

Figure 12: L_2-error (left), average Newton iterations per timestep per stage (middle) and average GMRES iterations per Newton iteration (right) for Euler equations with advection of density sine wave with $T_{end} = 0.8$ for the initial condition evaluated from the exact solution (39) using the SSP timestepping schemes. The plots are given for different timesteps Δt. The spatial discretization is set to $N_E = 16 \times 16$ and $N_p = 5$. A tolerance of $\varepsilon_{Newton} = 10^{-6}$ and $\varepsilon_{GMRES} = 10^{-3}$ is used, with a limit of 20 Newton iterations per implicit solve and 2000 GMRES iterations per Newton iteration. For the SSP-I2DRK45 scheme, the value of ε_{Newton} is set to 10^{-8} to avoid dominance of Newton error (only for $\Delta t = 0.025$). Note that the missing points on the plots indicate diverged solutions.

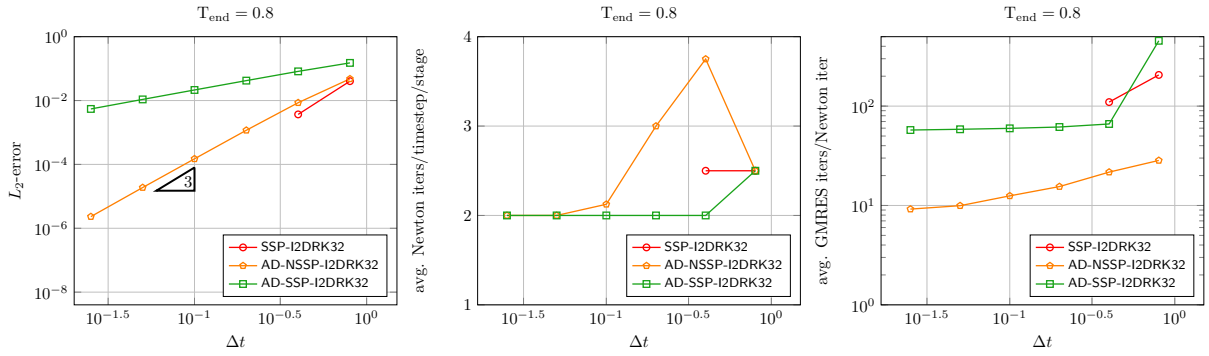

Figure 13: L_2-error (left), average Newton iterations per timestep per stage (middle) and average GMRES iterations per Newton iteration (right) for Euler equations with advection of density sine wave with $T_{end} = 0.8$ for the initial condition evaluated from the exact solution (39) using SSP-I2DRK32, AD-NSSP-I2DRK32 and AD-SSP-I2DRK32 schemes. The plots are given for different timesteps Δt. The spatial discretization is set to $N_E = 16 \times 16$ and $N_p = 5$. A tolerance of $\varepsilon_{Newton} = 10^{-4}$ and $\varepsilon_{GMRES} = 10^{-2}$ is used, with a limit of 20 Newton iterations per implicit solve and 2000 GMRES iterations per Newton iteration. Note that the missing points on the plots indicate diverged solutions.

SSP-I2DRK32 AD-SSP-I2DRK32 schemes. We consider the minimum of the wave speeds to compute l_Λ, which is necessary for the AD-SSP-I2DRK32 scheme. Using the explicit solution (39), we find that the minimum bound on the wave speeds

$$\min\{\mathbf{u} \cdot \mathbf{n}, \mathbf{u} \cdot \mathbf{n} \pm c\} = 0.3.$$

Since the minimum value of the wave speed is 0.3, we select the same value of $l_\Lambda = 0.9$ used for linear advection

equations. Similar to the findings in linear advection equations, the AD-SSP-I2DRK32 scheme provides stable solutions for the Euler equations with a reduction in error. However, the convergence order has decreased to almost one, likely due to the larger error constants.

4.3 Navier-Stokes equations

Next, we consider the two dimensional Navier-Stokes equations,

$$\mathbf{w}_t + \nabla \cdot \Big(\mathbf{F}^{\text{inv}}(\mathbf{w}) - \mathbf{F}^{\nu}(\mathbf{w}, \nabla \mathbf{w}) \Big) = 0, \tag{40}$$

with the state variables $\mathbf{w}$, the inviscid Euler flux $\mathbf{F}^{\text{inv}}$; and the viscous flux $\mathbf{F}^{\nu}$ given by

$$\mathbf{F}^{\nu}(\mathbf{w}, \nabla \mathbf{w}) = \begin{pmatrix} 0 \\ \tau \\ \tau.\mathbf{v} + \mathbf{q} \end{pmatrix} \tag{41}$$

where τ is the viscous tensor and $\mathbf{q}$ is the heat flux, given by

$$\tau := \mu\big(\nabla \mathbf{v} + (\nabla \mathbf{v})^T - \frac{2}{3}(\nabla \cdot \mathbf{v})\mathbf{Id}\big), \text{ and } \mathbf{q} := \lambda_T \nabla T, \tag{42}$$

respectively. The corresponding other parameters and constants used in the above equations are, dynamic viscosity μ, temperature T given by the ideal gas equation, thermal conductivity $\lambda_T = \frac{c_p \mu}{Pr}$, $Pr = 0.72$ is the fluid specific Prandtl number, specific heat capacity $c_p = \frac{R\gamma}{\gamma - 1}$ and the specific gas constant $R = \frac{1}{\gamma}$.

As the viscous flux $\mathbf{F}^{\nu}$ in the Navier-Stokes equations (40) depends on the state vector $\mathbf{w}$ as well as its gradient $\nabla \mathbf{w}$, it results into a second order PDE system. It is required to use an extended first order form for the equation (40) so as to utilize the fully discrete forms mentioned in the previous sections. Here, we use the BR2 lifting operator (see [1]) for the discretization of the second order equations. See [31, Sec. 5.1.1 - Sec. 5.1.3] for a detailed derivation.

For the numerical validation of the Navier-Stokes equations, we use the same set up as for the Euler equations. The viscosity is chosen to be $\mu = 10^{-3}$. In order to compute the L_2-error, a reference solution is computed via a fourth order explicit scheme [3] with a very small timestep $\Delta t = 10^{-6}$. The convergence results for the schemes are plotted in Fig. 14. The second order SSP scheme (SSP-I2DRK21) exhibit their desired order of convergence almost for every timesteps. However, the fourth order SSP scheme (SSP-I2DRK45) attains its actual order of convergence only for timesteps $\Delta t \leq 0.0125$. Even the second order schemes performs slightly better than the fourth order scheme for a couple of timesteps. The third order scheme (SSP-I2DRK32) diverges for timesteps $0.0125 \leq \Delta t \leq 0.1$ and provides stable solutions to other timesteps. Comparison of the linear and non-linear iterations for the Navier-Stokes equations for the three schemes in Fig. 14 shows a similar behavioral pattern as that of the Euler equations.

In Fig. 15, we present the convergence plots along with the average Newton and GMRES iterations required for implicit solves using the SSP-I2DRK32, AD-NSSP-I2DRK32 and AD-SSP-I2DRK32 schemes for the Navier-Stokes equations. Due to a lack of information regarding the distribution of eigenvalues for the spatially discretized advection-diffusion equation, we have chosen to use the minimum wave speed of $0.3 + \sqrt{2}$ from the hyperbolic part of the Navier-Stokes equation (40). Consequently, the value of $k_{\min}$ required for the AD-NSSP-I2DRK32 scheme is determined based on this wave speed bound of $0.3 + \sqrt{2}$, similar to the calculation used for the Euler equations.

The AD-NSSP-I2DRK32 scheme exhibits the desired convergence, requiring relatively few GMRES iterations compared to the SSP-I2DRK32 and AD-SSP-I2DRK32 schemes. For the AD-SSP-I2DRK32 scheme, we choose $l_\Lambda = 0.45$ heuristically. This scheme provides stable solutions for the Navier-Stokes equations with a reduction in error. The trend of order reduction observed in the Euler and linear advection equations is also evident here. However,

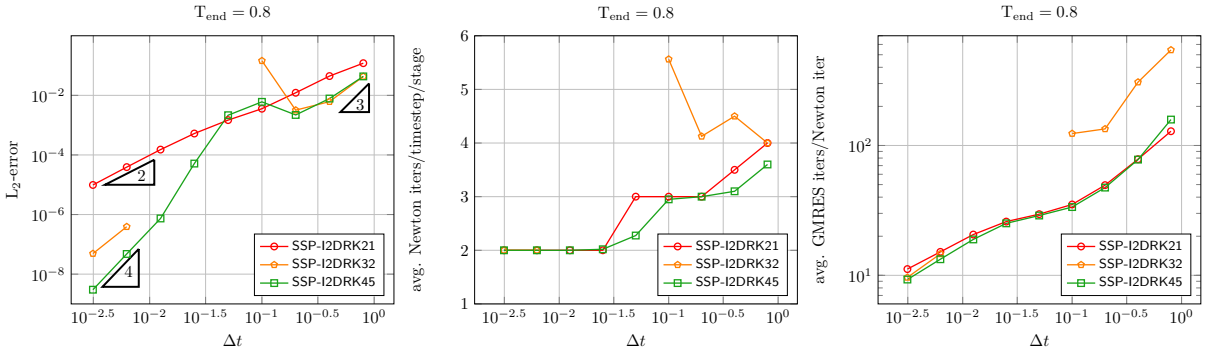

Figure 14: L_2-error (left), average Newton iterations per timestep per stage (middle) and average GMRES iterations per Newton iteration (right) for Navier-Stokes equations with advection and diffusion of density sine wave with $T_{end} = 0.8$ for the initial condition evaluated from the exact solution (39) using the SSP timestepping schemes. The plots are given for different timesteps Δt. The spatial discretization is set to $N_E = 16 \times 16$ and $N_p = 5$. A tolerance of $\varepsilon_{Newton} = 10^{-6}$ and $\varepsilon_{GMRES} = 10^{-3}$ is used, with a limit of 20 Newton iterations per implicit solve and 2000 GMRES iterations per Newton iteration. Note that the missing points on the plots indicate diverged solutions.

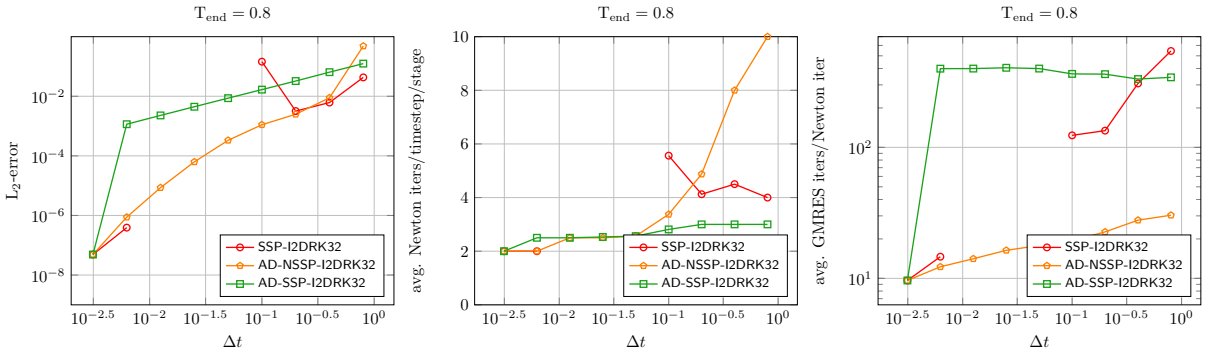

Figure 15: L_2-error (left), average Newton iterations per timestep per stage (middle) and average GMRES iterations per Newton iteration (right) for Navier-Stokes equations with advection and diffusion of density sine wave with $T_{end} = 0.8$ for the initial condition evaluated from the exact solution (39) using SSP-I2DRK32, AD-NSSP-I2DRK32 and AD-SSP-I2DRK32 schemes. The plots are given for different timesteps Δt. The spatial discretization is set to $N_E = 16 \times 16$ and $N_p = 5$. A tolerance of $\varepsilon_{Newton} = 10^{-6}$ and $\varepsilon_{GMRES} = 10^{-3}$ is used, with a limit of 20 Newton iterations per implicit solve and 2000 GMRES iterations per Newton iteration. Note that the missing points on the plots indicate diverged solutions.

the AD-SSP-I2DRK32 scheme requires more GMRES iterations per Newton iteration compared to the AD-NSSP-I2DRK32 scheme, which may be a consequence of smaller k values leading to a non-linear system.

For the fourth-order SSP scheme, we observed a significant deterioration in error reduction for timestep sizes ranging from 0.025 to 0.1. Since the SSP-I2DRK45 scheme is not A-stable, we further investigated stability in this context. We constructed a series of I2DRK45(α) schemes with varying stability angles α, maintaining the imaginary

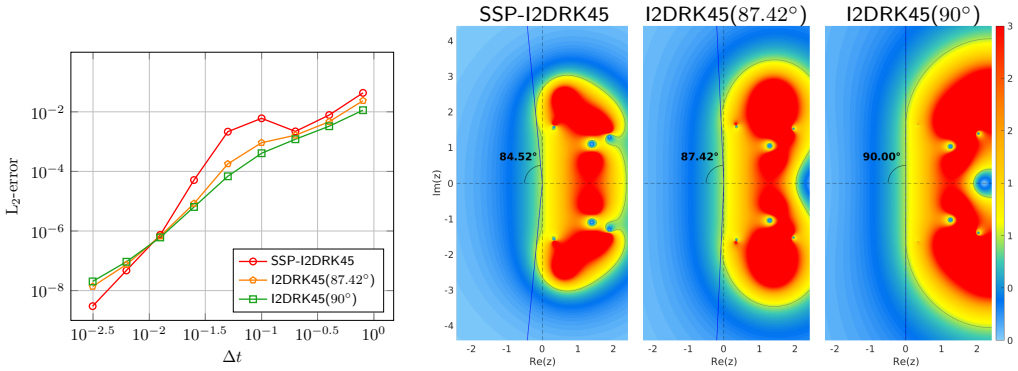

Figure 16: L_2-error (left) for Navier-Stokes equations with advection and diffusion of density sine wave with $T_{end} = 0.8$ for the initial condition evaluated from the exact solution (39) using SSP-I2DRK45, I2DRK45(87.42°) and I2DRK45(90°) schemes. The spatial discretization is set to $N_E = 16 \times 16$ and $N_p = 5$. A tolerance of $\varepsilon_{Newton} = 10^{-6}$ and $\varepsilon_{GMRES} = 10^{-3}$ is used, with a limit of 20 Newton iterations per implicit solve and 2000 GMRES iterations per Newton iteration. On the right, the stability angle and the stability region of the schemes SSP-I2DRK45, I2DRK45(87.42°) and I2DRK45(90°) are shown.

parts of the poles that cause instability at nearly the same positions. The detailed construction of the I2DRK45(α) schemes is provided in A.2.

In Fig. 16, we show the convergence plots for the SSP-I2DRK45, I2DRK45(87.42°), and I2DRK45(90°) schemes. It is clear that the I2DRK45(87.42°) and I2DRK45(90°) schemes show significant improvement compared to SSP-I2DRK45, consistently reducing errors for timestep sizes of $0.025 \leq \Delta t \leq 0.1$. Therefore, the results in Fig. 16 implies that the anomalies observed in the SSP-I2DRK45 scheme for the Navier-Stokes equations most likely stemmed from its instability.

5 Conclusion and outlook

In this work, we have analyzed the stability properties of the two-derivative SSP schemes [7], and have shown that the diagonally implicit two-derivative two-stage third order SSP can never be A-stable. SSP timestepping schemes [7] were implemented for Navier-Stokes equations in a DGSEM spatial framework. The complexity of the implementation of two-derivative Runge-Kutta scheme was outstripped by the introduction of the additional variable $\boldsymbol{\sigma}$ for the first order derivative as done in [26]. The stage values of non-linear equations were solved using Newton's method by employing GMRES method with a matrix-free approach on underlying preconditioned linear systems.

The second and fourth-order SSP schemes gave good convergence results on Euler and Navier-Stokes equations within a considerable number of Newton and GMRES iterations. The domination of temporal error over the spatial error for the chosen simulation setups was seen from the convergence plots. However, third-order SSP scheme encountered stability issues across a wide range of time step sizes due to the presence of poles of the stability function on the imaginary axis.

We have constructed and analyzed a family of A(α)-stable third-order schemes. The analysis reveals that the location of the unstable region in an A(α)-stable time-stepping scheme is more crucial than the stability angle. Based on the findings from the stability analysis, we have developed a stability adaptive third order SSP and non-SSP

schemes. The adaptive non-SSP scheme converged with the desired order for all test cases. Although the adaptive SSP scheme experienced an order reduction, it provided a stable solution in contrast to the original third-order SSP scheme. As we have devised a strategy to identify stable timestep sizes for A(α) schemes using eigenvalue bounds given in [19], it is possible to develop a hybrid SSP method that selectively incorporates higher-order SSP schemes to ensure both stability and overall accuracy.

While our analysis concentrates on a specific third-order method, the stabilizing techniques can be applied to a general class of two-derivative schemes. We also utilized these techniques to construct a series of A(α)-stable fourth-order schemes to investigate the anomalies observed in the fourth-order SSP scheme when applied to the Navier-Stokes equations. Numerical results showcased the importance of requiring A-stable time-stepping schemes when simulations are conducted over large final times, particularly for stiff systems.

There are four possible directions for future investigations. First, we are interested in implementing the asymptotic preserving IMEX timestepping schemes for low-Mach problems combined with DGSEM spatial discretization. Second, incorporation of the higher derivatives (order greater than two) using the Jacobian-free methods [4] and hence more flexibility can be achieved over the coefficients. Third, since there are higher-order strong stability preserving GLMs in literature [23, 21, 22], the implementation of these schemes into the DGSEM framework is subject to numerical investigations. Lastly, as there are only limited studies on strong stability preserving deferred correction schemes [20], investigating SSP-HBPC schemes is another potential direction for future research.

Acknowledgments

Arjun Thenery Manikantan was funded by the "Bijzonder Onderzoeksfonds" (BOF) from UHasselt - project no. BOF21KP12. Jonas Zeifang was funded by the Deutsche Forschungsgemeinschaft (DFG, German Research Foundation) - project no. 457811052. We acknowledge the VSC (Flemish Supercomputer Center) for providing computing resources. The VSC is funded by the Research Foundation - Flanders (FWO) and the Flemish Government.

A Construction of reference schemes

A.1 The third-order I2DRK32(79.94°) scheme

The ξ-I2DRK32 schemes are constructed by keeping the implicit term of the first derivative (a_{11}) in the first stage as a free variable ξ. Using the order conditions [7, Sec. 2.1, p=1, 2, 3], the remaining coefficients were written as a function of ξ. Hence we have the Butcher coefficients for the two-derivative two-stage third order Runge-Kutta scheme ξ-I2DRK32

$$\mathbf{A} = \begin{bmatrix} \xi & 0 \\ 0 & 1 \end{bmatrix} \text{ and } \dot{\mathbf{A}} = \begin{bmatrix} -\frac{1}{6} & 0 \\ -\frac{1}{6(1-\xi)} & -\frac{1}{2} + \frac{1}{6(1-\xi)} \end{bmatrix}, \tag{43}$$

with $\xi \neq 1$. The ξ-I2DRK32 are A(α)-stable schemes.

The I2DRK32(79.94°) scheme is constructed to have the same stability angle as that of an SSP-I2DRK32 scheme. The scheme is obtained via slightly tuning the $\frac{1}{60}$-I2DRK32 scheme with a different coefficient $\dot{a}_{11} = -\frac{100}{6307}$. Hence the Butcher coefficients for two-derivative two-stage third order I2DRK32(79.94°) scheme is given by

$$\mathbf{A} = \begin{bmatrix} \frac{1}{60} & 0 \\ 0 & 1 \end{bmatrix} \text{ and } \dot{\mathbf{A}} = \begin{bmatrix} -\frac{100}{6307} & 0 \\ -\frac{10}{59} & -\frac{39}{118} \end{bmatrix}. \tag{44}$$

A.2 The fourth-order I2DRK45(α) schemes

For the SSP-I2DRK45 scheme, it was observed that the pole of the stability function

$$\mathcal{S}(z) = \frac{1 + \sum_{j=1}^{4} \left(a_{5j} z + \dot{a}_{5j} z^2\right) \mathcal{S}_j(z)}{\left(1 - a_{55} z - \dot{a}_{55} z^2\right)}$$

that is responsible for instability arise from the fourth stage

$$\frac{1}{1 - a_{44} z - \dot{a}_{44} z^2}. \tag{45}$$

To have a pole at the point $z = q \pm mi$ for Eq. (45), it is sufficient to choose the following coefficients

$$\begin{aligned} a_{44} &= \frac{2q}{q^2 + m^2}, \\ \dot{a}_{44} &= \frac{-1}{q^2 + m^2}. \end{aligned} \tag{46}$$

The poles of the Eq. (45) for the SSP-I2DRK45 scheme with coefficients $a_{44} = 0.191388711018110$ and $\dot{a}_{44} = -0.161628266349058$ is

$$q \pm mi \approx 0.592064480246234 \pm 2.4158841558212118i.$$

We construct I2DRK45(α) schemes by fixing $m \approx 2.4158841558212118$ and varying the real part q using the relationship given in Eq. (46). The coefficients a_{ii} and $\dot{a}_{ii}$ for $i \neq 4$ are taken directly from the Butcher tableau of the SSP-I2DRK45 scheme. The remaining lower diagonal coefficients a_{ij} and $\dot{a}_{ij}$ for $i < j$ are determined by solving order equations to achieve fourth-order accuracy.

The values of q corresponding to the schemes I2DRK45(87.42°) and I2DRK45(90°) are 1.4 and 2.5, respectively. The I2DRK45(α) scheme shows a trend of increasing stability angle α as q is increased. See, Fig. 16 for the stability regions.

Declarations

Conflict of interest The authors declare no competing interests

References

[1] F. Bassi, S. Rebay, G. Mariotti, S. Pedinotti, and M. Savini. A high-order accurate discontinuous Finite Element method for inviscid and viscous turbomachinery flows. *Proceedings of 2nd European Conference on Turbomachinery, Fluid Dynamics and Thermodynamics*, pages 99–108, 1997.

[2] Francesco Bassi, L. Botti, A. Colombo, Antonio Ghidoni, and F. Massa. Linearly implicit Rosenbrock-type Runge-Kutta schemes applied to the discontinuous Galerkin solution of compressible and incompressible unsteady flows. *Computers and Fluids*, 118:305–320, 09 2015.

[3] M.H. Carpenter and C.A. Kennedy. Fourth-order 2N-storage Runge-Kutta schemes. Technical report, NASA Langley Research Center, 1994.

[4] Jeremy Chouchoulis, Jochen Schütz, and Jonas Zeifang. Jacobian-free explicit multiderivative Runge–Kutta methods for hyperbolic conservation laws. *Journal of Scientific Computing*, 90(3):96, Feb 2022.

[5] Andrew J. Christlieb, Sigal Gottlieb, Zachary J. Grant, and David C Seal. Explicit strong stability preserving multistage two-derivative time-stepping schemes. *Journal of Scientific Computing*, 68:914–942, 2016.

[6] M. Franciolini, A. Crivellini, and A. Nigro. On the efficiency of a matrix-free linearly implicit time integration strategy for high-order discontinuous Galerkin solutions of incompressible turbulent flows. *Computers & Fluids*, 159:276–294, 2017.

[7] Sigal Gottlieb, Zachary J. Grant, Jingwei Hu, and Ruiwen Shu. High order strong stability preserving multiderivative implicit and IMEX Runge–Kutta methods with asymptotic preserving properties. *SIAM Journal on Numerical Analysis*, 60(1):423–449, 2022.

[8] Sigal Gottlieb, Chi-Wang Shu, and Eitan Tadmor. Strong stability-preserving high-order time discretization methods. *SIAM Review*, 43(1):89–112, 2001.

[9] Zachary Grant, Sigal Gottlieb, and David C. Seal. A strong stability preserving analysis for explicit multistage two-derivative time-stepping schemes based on Taylor series conditions. *Communications on Applied Mathematics and Computation*, 1(1):21–59, 2019.

[10] E. Hairer and G. Wanner. Multistep-multistage-multiderivative methods for ordinary differential equations. *Computing (Arch. Elektron. Rechnen)*, 11(3):287–303, 1973.

[11] E. Hairer and G. Wanner. *Solving ordinary differential equations II.* Springer Series in Computational Mathematics, 1991.

[12] Ralf Hartmann, Francesco Bassi, Igor Bosnyakov, Lorenzo Botti, Alessandro Colombo, Andrea Crivellini, Matteo Franciolini, Tobias Leicht, Emeric Martin, Francescocarlo Massa, et al. Implicit methods. In *TILDA: Towards Industrial LES/DNS in Aeronautics*, pages 11–59. Springer, 2021.

[13] F. Hindenlang, G. Gassner, C. Altmann, A. Beck, M. Staudenmaier, and C.-D. Munz. Explicit discontinuous Galerkin methods for unsteady problems. *Computers & Fluids*, 61:86–93, 2012.

[14] Alexander Jaust, Jochen Schütz, and David C. Seal. Implicit multistage two-derivative discontinuous Galerkin schemes for viscous conservation laws. *Journal of Scientific Computing*, 69:866–891, 2016.

[15] K. Kaiser and J. Schütz. A high-order method for weakly compressible flows. *Communications in Computational Physics*, 22(4):1150–1174, 2017.

[16] D. A. Knoll and D. E. Keyes. Jacobian-free Newton–Krylov methods: a survey of approaches and applications. *Journal of Computational Physics*, 193:357–397, 2004.

[17] D. A. Kopriva. *Implementing spectral methods for partial differential equations: Algorithms for scientists and engineers.* Springer Science & Business Media, 2009.

[18] Nico Krais, Andrea Beck, Thomas Bolemann, Hannes Frank, David Flad, Gregor Gassner, Florian Hindenlang, Malte Hoffmann, Thomas Kuhn, Matthias Sonntag, et al. FLEXI: A high order discontinuous Galerkin framework for hyperbolic–parabolic conservation laws. *Computers & Mathematics with Applications*, 81:186–219, 2021.

[19] Lilia Krivodonova and Ruibin Qin. An analysis of the spectrum of the discontinuous galerkin method. *Applied Numerical Mathematics*, 64:1–18, 2013.

[20] Yuan Liu, Chi-Wang Shu, and Mengping Zhang. Strong stability preserving property of the deferred correction time discretization. *Journal of Computational Mathematics*, 26(5):633–656, 2025/05/23/ 2008. Full publication date: September 2008.

[21] Afsaneh Moradi, Ali Abdi, and Javad Farzi. Strong stability preserving second derivative general linear methods with Runge–Kutta stability. *Journal of Scientific Computing*, 85(1):1, Sep 2020.

[22] Afsaneh Moradi, Ali Abdi, and Gholamreza Hojjati. Strong stability preserving implicit and implicit–explicit second derivative general linear methods with RK stability. *Computational and Applied Mathematics*, 41(4):135, Apr 2022.

[23] Afsaneh Moradi, Javad Farzi, and Ali Abdi. Strong stability preserving second derivative general linear methods. *Journal of Scientific Computing*, 81(1):392–435, Oct 2019.

[24] N. C. Nguyen, J. Peraire, and B. Cockburn. High-order implicit hybridizable discontinuous Galerkin methods for acoustics and elastodynamics. *Journal of Computational Physics*, 230:3695–3718, 2011.

[25] J. Schütz and D. Seal. An asymptotic preserving semi-implicit multiderivative solver. *Applied Numerical Mathematics*, 160:84–101, 2021.

[26] J. Schütz, D.C. Seal, and A. Jaust. Implicit multiderivative collocation solvers for linear partial differential equations with discontinuous Galerkin spatial discretizations. *Journal of Scientific Computing*, 73:1145–1163, 2017.

[27] Jochen Schütz, David C Seal, and Jonas Zeifang. Parallel-in-time high-order multiderivative IMEX solvers. *Journal of Scientific Computing*, 90(54):1–33, 2022.

[28] A. H. Stroud and D. D. Stancu. Quadrature formulas with multiple Gaussian nodes. *SIAM Journal on Numerical Analysis*, 2:129–143, 1965.

[29] P Turán. On the theory of the mechanical quadrature. *Acta Universitatis Szegediensis Acta Scientiarum Mathematicarum*, 12:30–37, 1950.

[30] J. Zeifang, J. Schütz, and D. Seal. Stability of implicit multiderivative deferred correction methods. *BIT Numerical Mathematics*, 2022.

[31] Jonas Zeifang and Jochen Schütz. Implicit two-derivative deferred correction time discretization for the discontinuous Galerkin method. *Journal of Computational Physics*, 464:111353, 2022.

[32] Jonas Zeifang, Arjun Thenery Manikantan, and Jochen Schütz. Time parallelism and Newton-adaptivity of the two-derivative deferred correction discontinuous Galerkin method. *Applied Mathematics and Computation*, 457:128198, 2023.

UHasselt Computational Mathematics Preprint Series

www.uhasselt.be/cmat